BAMS Article

Tropical Cyclones and Climate Change

Global Landfall Frequency Projections Derived from Knutson et al.

Stephen Jewson

ABSTRACT: Projections of changes in tropical cyclone (TC) characteristics under climate change are of great interest to those affected by TCs. In a recent paper, Knutson et al. combined a large number of previous results to produce projections consisting of distributions of possible future TC frequencies, intensities, and rainfall rates. These distributions provide a great resource for users of TC information. However, to apply the distributions to impacts models may require the user to solve a number of technical challenges including modeling correlations, fitting distributions, interpolation, and converting the projections to properties at landfall. I consider the frequency and intensity changes, and implement solutions for each of these challenges using a combination of recently published research and a new methodology. This allows me to produce a dataset of TC projections that give frequency changes as a function of landfall region and intensity. Mean intensity changes can then be derived from frequency changes. The projections are presented in a format that allows them to be used in impacts models without further processing. The interpolation and landfall adjustments tend to increase the frequency changes. As a result, my projections give increasing mean frequencies of hurricane-strength landfalling TCs in four out of six global basins, with mean frequencies increasing by up to 16% for a 2°C increase in global mean surface temperature. My projections are highly uncertain, but include uncertainty estimates. They are designed to be a useful resource for anyone interested in possible future TC frequencies and intensities.

KEYWORDS: Hurricanes/typhoons; Tropical cyclones; Climate change; Risk assessment; Insurance; Societal impacts

https://doi.org/10.1175/BAMS-D-22-0189.1
Corresponding author: Stephen Jewson, stephen.jewson@gmail.com
Supplemental material: https://doi.org/10.1175/BAMS-D-22-0189.2

In final form 10 April 2023

AFFILIATION: Jewson—Lambda Climate Research, London, United Kingdom

Tropical cyclones (TCs) cause great amounts of damage in many parts of the world. Normalized estimates for the damage caused by historical Atlantic hurricanes in the United States have been given by Weinkle et al. (2018) and Martinez (2020), and suggest average annual damages in 2018 terms of $16.7 billion and $26.5 billion (U.S. dollars), respectively. Normalized estimates for the damage caused by northwest Pacific typhoons in China by Chen et al. (2018) suggest average annual damages in 2015 terms of $15.4 billion (U.S. dollars). Given these large damages, a critical question for those affected by TCs is therefore how TC characteristics may have changed, or may change in the future, due to climate change. Recent research has considered many possible aspects of changes in TC characteristics due to climate change, including changes in their spatial distribution (Murakami et al. 2020), frequency and intensity (Emanuel 2020), landfall frequency (Knutson et al. 2022), intensity (Bhatia et al. 2019), size (Sun et al. 2017), rainfall rate (Liu et al. 2019; Stansfield et al. 2020), trajectories (Colbert et al. 2013; Garner et al. 2021), forward speed (Zhang et al. 2020; Hassanzadeh et al. 2020; Yamaguchi et al. 2020), and risk (Bloemendaal et al. 2022). This wealth of research is potentially very useful for those affected by TCs. However, precisely because of the large amount of research that has been published, many users of TC information struggle to know which TC studies to consider in their impacts models. They also struggle to deal with the often large differences in results between different studies. In addition, they may struggle with technical issues related to how to interpret published results in a way that is relevant for impacts models.

In a groundbreaking review paper, Knutson et al. (2020, henceforth K2020) combined results from a large number of different TC studies to produce distributions of change that give the range of results from the different studies. The distributions correspond to a 2°C increase in global mean surface temperature. They applied their approach to results for changes in the frequencies of Saffir–Simpson-scale category 0–5 storms [i.e., storms with lifetime maximum wind speed of 34 kt (1 kt ≈ 0.51 m s^{-1}) or greater, henceforth cat05 storms], frequencies of Saffir–Simpson-scale category 4–5 storms (i.e., storms with lifetime maximum wind speed of 113 kt or greater, henceforth cat45), mean intensity, and rainfall rate, for the six main TC ocean basins (North Atlantic, Northwest Pacific, East Pacific, North Indian, South Indian, and South Pacific). The K2020 distributions provide a useful standardized set of results that, for the variables considered, help provide possible resolutions to the questions of which studies to consider and how to deal with differences between results from different studies. Over time, as new studies appear and less accurate studies become less relevant, the distributions of results given by K2020 can be updated.

However, using the K2020 distributions in TC impacts models is not necessarily straightforward in practice for a number of reasons. For instance, in K2020:

- Results are presented as separate distributions of change for four variables, without discussion of correlations between the changes for the different variables. Users have to make correlation assumptions, and different correlation assumptions may lead to different downstream implications.

- Results are presented as quantiles and require additional processing to be able to simulate a distribution of values, as would be preferred for use in stochastic impact models.
- Including changes in mean intensity in addition to changes in cat05 and cat45 frequencies duplicates information. As a result, care has to be taken not to adjust an impacts model with the same information twice.
- The cat05 and cat45 intensity ranges overlap, and may need to be converted to changes in frequencies of cat03 and cat45 storms before they can be applied.
- No information is provided with regard to the relative changes in storm frequencies within the cat03 and cat45 intensity ranges. Different assumptions about how frequencies may change within the cat03 and cat45 ranges may lead to very different implications.
- Results are presented as changes in frequencies as a function of lifetime maximum intensity, while most impacts are related to landfalling intensities.

I have investigated how these issues can be resolved in a recent series of research projects (Jewson 2021, 2022a,b, henceforth J2022a and J2022b). In this article I apply the learnings from this research, along with a new methodology for relating lifetime maximum intensity to landfall intensity. I generate adjusted TC frequency projections that are designed for use in impacts models. My projections also correspond to a 2°C increase in global mean surface temperature and cover all six major TC basins. The basins are further subdivided into 18 regions to capture within-basin variations in the relationship between lifetime maximum intensity and landfall intensity. The projections can be incorporated straightforwardly into most impacts models by simulating from the provided distributions. My analysis is based on the K2020 projections and the International Best Track Archive for Climate Stewardship (IBTrACS). IBTrACS is a dataset of historical global TC observations, and contains data from many sources. I use the "U.S. Representative Agency" data in all basins, for consistency, but also include a sensitivity test which explores how the different sources in IBTrACS can lead to different results because of discrepancies between the different sources (Bai et al. 2023). Both the K2020 projections and the IBTrACS data are described in more detail in appendix A.

To generate landfall projections, I make various assumptions. The most important of these assumptions is the assumption that changes in frequencies as a function of landfall intensity can be derived from the K2020 changes in frequencies as a function of lifetime maximum intensity. This assumption implicitly assumes that TC genesis regions and TC trajectories will not change in such a way as to change landfall frequencies. This assumption is almost definitely not perfectly valid, and there have been several studies which have suggested that genesis regions and trajectories may change (Colbert et al. 2013; Garner et al. 2021; Knutson et al. 2022). The understanding of these changes is, however, at an early stage and based on a limited number of studies. I have not tried to use these results to inform my calculations of possible landfall frequency changes.

My methodologies for adjusting the K2020 results are statistical, rather than based on numerical climate models. Ultimately, climate models will likely prove to be the best tool for understanding all aspects of changes in TC behavior, including landfalling frequencies, and when appropriate climate model studies become available, they will likely supersede statistical approaches.

Distributions, correlations, and interpolation

Fitting continuous distributions to the K2020 quantiles. The first step of my methodology involves fitting lognormal distributions to the K2020 quantiles for the cat05 and cat45 frequency changes in each basin. It also involves determining an appropriate correlation between the two distributions, and deriving a distribution for the fractional changes for

cat03 storm frequencies. Fitting continuous distributions to the quantiles allows for smooth interpolation and extrapolation of the distributions of change. It also condenses the results for each variable into just two parameters, which facilitates the communication of the results, and makes it straightforward for users of the data to simulate from the fitted distributions. Using the lognormal captures the appropriate range of multiplicative changes, from zero to infinity. Determining a correlation value allows me to simulate from the two distributions in an appropriately correlated way. Presenting results as changes in cat03 and cat45 frequencies simplifies the application of the results to many kinds of impacts models. A detailed discussion of these steps is given in appendix B. Correlations are determined from the requirement that the K2020 frequency and mean intensity changes should be consistent. Changes in cat03 storm frequencies are determined by converting cat05 and cat45 changes into the absolute number of storms using historical frequencies, before calculating the difference and converting back to relative changes.

As an example, results showing the K2020 quantiles and fitted quantiles from the lognormal distribution for the North Indian Ocean are given in Figs. 1a and 1b. Corresponding figures for the other five basins are given in the online supplemental material (https://doi.org/10.1175/BAMS-D-22-0189.2). In all basins, the fitted quantiles lie within the 95% confidence intervals around the K2020 quantiles. The correlation modeling implies that the rank correlation between the two distributions should be set to 1. This correlation allows me to generate simulations of cat05 and cat45 frequency changes from which I derive simulations of the fractional changes in cat03 frequencies using historical frequencies from IBTrACS. The cat03 changes derived in this way have a rank correlation of 1 with the cat05 and cat45 changes. I also fit lognormal distributions to the cat03 changes. The fit is good for all basins, with all Q–Q correlations above 0.995. For the North Indian Ocean example, the simulated and fitted distributions for cat03 changes are illustrated in Fig. 1c, and for other basins in the supplemental material. The parameter values for the fitted distributions for cat03 and cat45 frequency changes are given in the supporting data (Jewson 2022c). Given these fitted distributions, and correlation values, I can simulate an arbitrary number of climate outcomes as correlated pairs of changes in cat03 and cat45 frequencies.

Interpolating changes within the cat03 and cat45 ranges. The K2020 results give distributions of changes for cat05 and cat45 frequencies, from which I have derived a distribution of changes for cat03 frequencies as described above. To use the cat03 and cat45 frequency changes in an impacts model, a user must decide what assumptions to make about changes to the frequencies within the cat03 and cat45 ranges. For example, should they change cat0 frequencies in the same way that they change cat3 frequencies? Perhaps the most obvious method for defining changes of frequencies within the cat03 and cat45 ranges is a "step" model, in which the frequency changes are assumed to be constant within the cat03 and cat45 ranges, with a step change between cat3 and cat4. This step change could, however, be considered physically unrealistic. Also, in observed TC frequency distributions, the frequency of cat03 storms is dominated by the frequencies of cat02 storms. For instance, in the IBTrACS data I am using, only 9% of the cat03 storms are cat3. To the extent that climate models show similar frequency distributions, climate model cat03 results may well not, therefore, represent cat3 storm frequency changes particularly well. Given this, an obvious alternative to the step model is a "linear" model, in which the fractional changes in frequency are assumed to vary linearly with intensity. This avoids the step change. In reality, neither the step model or the linear model is likely to be correct. More complex models could be considered, but without good justification they would be largely arbitrary. A key priority for further research is to understand in more detail how climate change affects the frequency of TCs of different intensities.

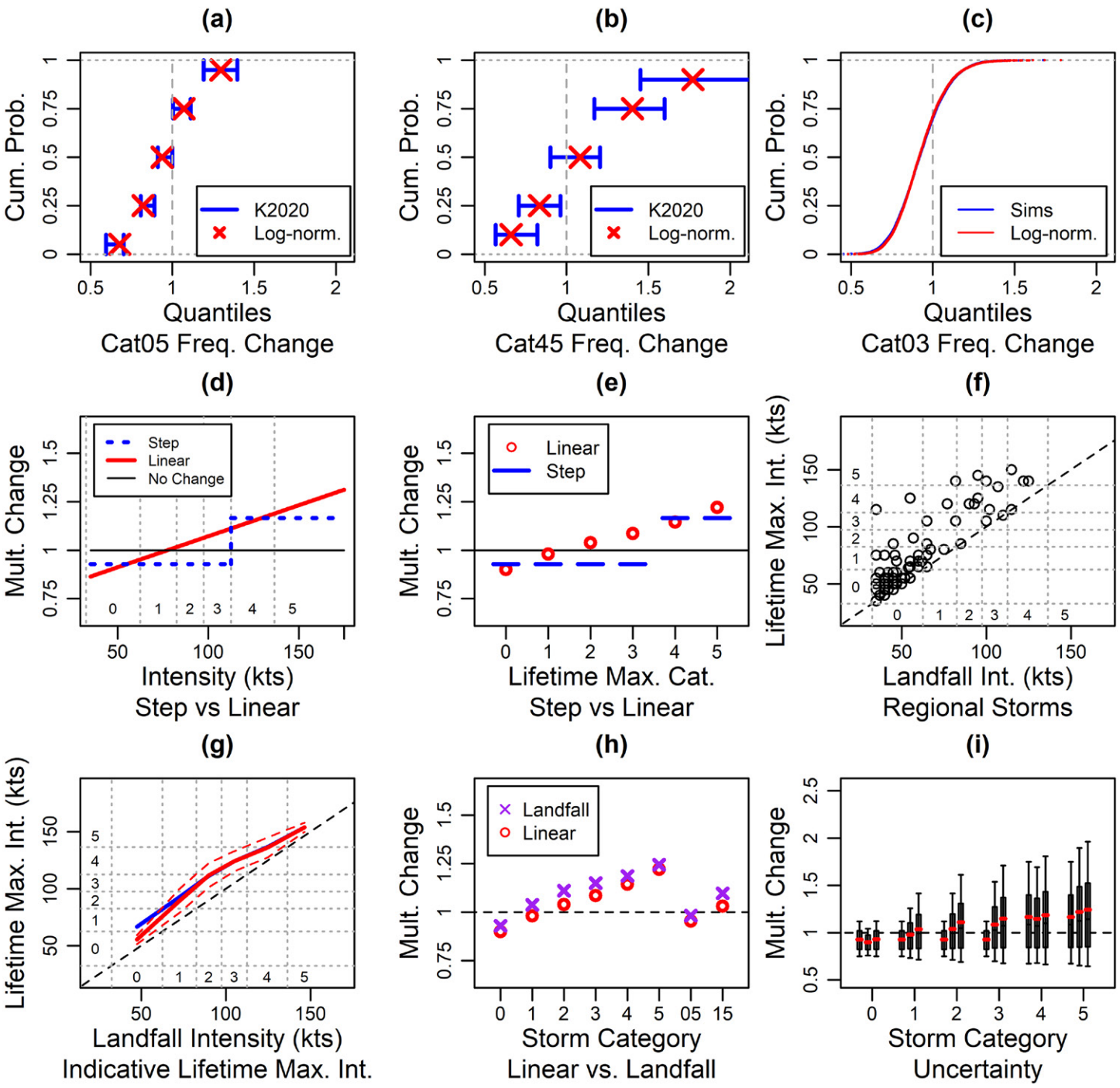

Fig. 1. Results from the various steps of my analysis of tropical cyclone frequencies in the Bay of Bengal, as an example of the analysis I have applied to 18 global regions. (a) Quantiles of change for cat05 storms from K2020 (blue error bars show the 95% confidence limits around the K2020 results), and the corresponding quantiles for a fitted lognormal distribution (red crosses). (b) As in (a), but for cat45 storms. (c) Distribution of changes in cat03 storms, calculated from the data in (a) and (b) combined with IBTrACS data (blue line, mostly obscured by the red line), and a fitted lognormal distribution (red line). (d) Mean multiplicative changes in storm frequency vs storms intensity, for step and linear models. (e) As in (d), but vs storm category. (f) Lifetime maximum intensity and the landfall intensity of every landfalling cat05 storm from IBTrACS in this region, for the period 1980–2021. (g) Expected lifetime maximum intensities calculated as described in the text, global values (blue solid line), and regional values for the Bay of Bengal (red solid line), with sampling uncertainty for the regional values, given by plus and minus two standard deviations (red dashed lines). (h) Mean multiplicative frequency changes for landfall storms, based on the linear model without landfall adjustment (red circles), and with landfall adjustment (purple crosses), vs storm category, including cat05 and cat15. (i) Distribution of multiplicative frequency changes for storms, based on three stages of the modeling process, for each category. The three stages are the step model, the linear model, and the landfall model. The step model and linear models apply to lifetime maximum intensities while the landfall model applies to landfall intensities.

Deciding whether to use a step or linear model can have large downstream impacts. For instance, for the United States, the Weinkle et al. (2018) normalized hurricane losses suggest that cat3 and cat4 storms are the biggest contributors to average annual damages due to hurricanes. Cat5 storms cause more damage individually than cat4 storms, but are so much less common that they contribute less to average annual damage. Cat0, 1, and 2 storms are more common than cat3 storms, but cause so much less damage individually that they also contribute less to average annual damage. As a result of the large impact of cat3 and cat4 storms, final average annual damage estimates are highly sensitive to any modeling decisions related to the frequency changes of cat3 and cat4 storms, such as the choice of whether to use the step or linear models.

J2022a were able to show that the linear model gives a better overall fit to the K2020 quantiles than the step model. Given this result, I use the linear model in my analysis. I apply it separately to every pair of simulations of cat03 and cat45 frequencies, thus creating a large ensemble of different linear models for each basin. These different linear models capture the uncertainty ranges in the K2020 results.

Figure 1d illustrates the mean linear model for the North Indian Ocean example, compared with the mean step model, as a function of intensity in knots. In this case, the mean step model gives decreases in the frequency of cat2 and cat3 storms, while the mean linear model gives increases. Cat0 and cat1 storms decrease in frequency in both models. The linear model is fitted so that the overall percentage changes in the number of cat03 and cat45 storms are the same in the two models, even though that may not appear to be the case in Fig. 1d. The overall percentage change is given by the changes in Fig. 1d weighted by the different frequencies of storms in each intensity category, with cat0 storms being much more frequent than cat2 and cat3 storms.

Figure 1e shows the step and linear models, now as a function of storm category, and showing mean changes within each category. The linear model is no longer precisely linear, when considered as a function of storm category, because of the irregular spacing of the boundaries in the Saffir–Simpson scale. For cat2 and cat3 storms, the step model can again be seen to give decreases in frequency, while the linear model gives increases. Corresponding figures for other basins are given in the supplemental material.

Adjustment for landfall

Regional variations in landfall behavior. The K2020 results give frequency changes as a function of storm lifetime maximum intensity. However, for many applications, it is more useful to present frequency changes as a function of storm landfall intensity. The landfall intensity can never be higher than the lifetime maximum intensity, and is often lower. For example, many storms with a lifetime maximum intensity of cat4 or cat5 may make landfall as cat3 or weaker. I assume that when the K2020 results suggest that cat4 or cat5 storms will increase in frequency, landfalling storms that were previously cat4 or cat5 will also increase in frequency, whatever their intensity at landfall. This concept is the basis for my landfall adjustments. Previous work, looking at the Atlantic (J2022b), found that the statistical relationship between lifetime maximum intensities and landfall intensities varies regionally within the Atlantic basin (this work is discussed in detail in appendix C). For instance, storms that make landfall in the Gulf of Mexico typically have landfall intensities only slightly below their lifetime maximum intensity, whereas the difference between landfall intensities and lifetime maximum intensities for storms that make landfall in the Lesser Antilles is much larger. This relates to the differing life cycles of storms in these regions. Given the regional variations in the relationship between lifetime maximum intensity and landfall intensity, the first stage in my landfall adjustment approach is to define regions in which to derive different landfall adjustments. A detailed discussion of how I chose the regions is also given in appendix C. This discussion leads me to define the 18 regions

Table 1. The 18 regions used in this study.

Region number	Basin	Region name	Region description
1	North Atlantic	Gulf of Mexico and Central America	Central America east coast, U.S. Gulf Coast
2	North Atlantic	Central Caribbean	Central Caribbean Islands
3	North Atlantic	Lesser Antilles	Lesser Antilles
4	North Atlantic	North America east coast	U.S. and Canada east coast
5	Northwest Pacific	China west	China west of 113.7°E
6	Northwest Pacific	China east	Chine east of 113.7°E
7	Northwest Pacific	Japan+	Japan and extension
8	Northwest Pacific	Philippines+	Philippines and extension
9	Northwest Pacific	South Korea+	South Korea and extension
10	Northwest Pacific	Taiwan+	Taiwan and extension
11	Northwest Pacific	Vietnam+	Vietnam and extension
12	East Pacific	East Pacific west	Hawaii and North America west coast north of 22°N
13	East Pacific	East Pacific east	North America west coast south of 22°N
14	North Indian	Arabian Sea	North Indian Ocean west of 77.5°E
15	North Indian	Bay of Bengal	North Indian Ocean east of 77.5°E
16	South Indian	Indian Ocean Southwest	South Indian Ocean west of 77.5°E
17	South Indian	Indian Ocean Southeast	South Indian Ocean from 77.5° to 137°E
18	South Pacific	South Pacific	South Pacific

listed in Table 1 and illustrated in Fig. 2. Precise polygon definitions of these regions are given in the supporting data.

A scatterplot of the observed landfall and lifetime maximum intensities for region 15, the Bay of Bengal, is given in Fig. 1f, for storms of cat0 and higher intensities. We see that for some storms, lifetime maximum intensity and landfall intensity are equal, but for most, lifetime maximum intensity exceeds landfall intensity. In some cases, lifetime maximum intensity is much higher. For example, there are two cat4 storms that made landfall as cat0.

Lifetime maximum intensity and landfall intensity modeling. Given the region definitions, I use historical storm data to model the relationship between landfall intensity and lifetime

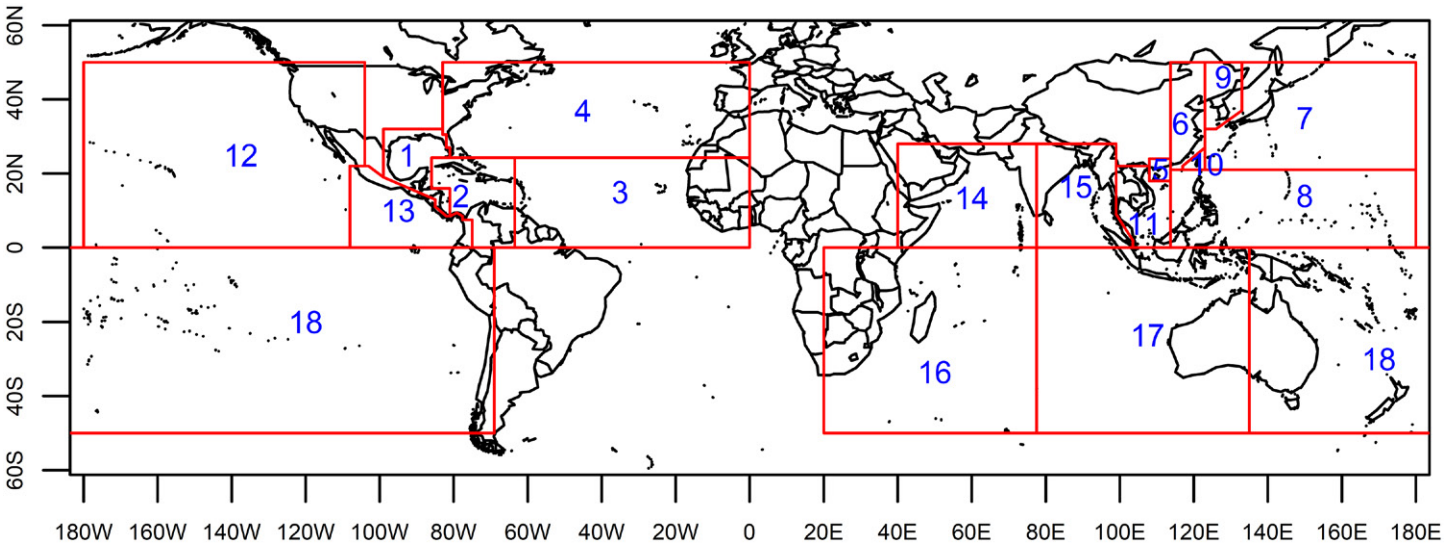

Fig. 2. The 18 regions used in this study. Names are given in Table 1, and precise polygon definitions are given in the supporting data.

maximum intensity, as a function of region. The goal of this modeling is to derive functions that give the expected lifetime maximum intensity (ELMI) of storms as a function of their landfall intensity category. I derive different ELMI functions for each region, by combining global and regional information, and by smoothing as a function of intensity. Details of the calculation are given in appendix D, and resulting function values are available in the supporting data.

Figure 3 shows lifetime maximum intensity and landfall intensity for all historical storms globally, along with the global ELMI values from my modeling. The global ELMI shows that storms are on average 1 or 2 categories more intense in terms of lifetime maximum intensity than landfall intensity.

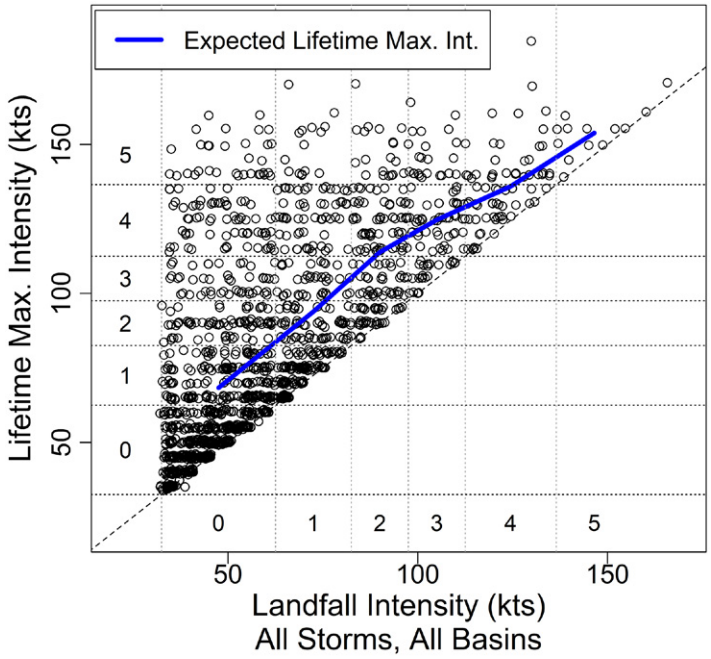

Fig. 3. Storm intensities for all cat0 and above landfalling storms in IBTrACS for the period 1980–2021. The horizontal axis shows landfall intensity and the vertical axis shows lifetime maximum intensity, both in knots, with Saffir–Simpson categories indicated inside the plot. A small amount of noise is added to avoid overlapping points, since many combinations of landfall and lifetime maximum intensity are duplicated, especially for weaker storms. The blue line shows the expected lifetime maximum intensity, as a function of landfall intensity, and was calculated by averaging the intensities of storms in each landfall intensity bin.

Figure 4 shows lifetime maximum intensity versus landfall intensity scatterplots for all 18 regions. It also shows the global and regional ELMI values. The North America east coast, China W, Philippines+, Taiwan+, Vietnam+, Arabian Sea, and South Pacific regions show regional ELMI values close to the global ELMI values. However, a number of other regions show regional ELMI values that are noticeably different from the global values. For instance, South Korea+ shows regional ELMI values that are higher than the global ELMI values for cat0, 1, and 2, which are the only landfall intensities for which there are historical data in this region. The regional ELMI values are higher than the global ELMI values because almost all storms make landfall at an intensity much lower than their lifetime maximum intensity in South Korea+. The central Caribbean, Lesser Antilles, China east, Japan+, and East Pacific west regions also show regional ELMI values that are higher than the global ELMI values, to a greater or lesser extent depending on the region. The East Pacific east region, on the other hand, shows regional ELMI values lower than the global ELMI values for cat0, 1 and 2, which is the intensity range for most landfalling storms in this region. The lower regional ELMI values occur because most storms in this landfall intensity range make landfall at an intensity the same as, or only slightly lower than, their lifetime maximum intensity in this region. The Gulf of Mexico and Central America, Bay of Bengal, Indian southwest, and Indian southeast regions also show regional ELMI values that are lower than the global ELMI values, to a greater or lesser extent depending on the region. Figure 1g shows the global and regional ELMI values for the Bay of Bengal region, and also shows uncertainty around the regional ELMI values. This uncertainty is the standard error uncertainty due to the finite sample sizes used to derive the ELMI, and varies by region because of the varying sample sizes. This uncertainty is propagated into the subsequent analysis: details are given in appendixes D and E.

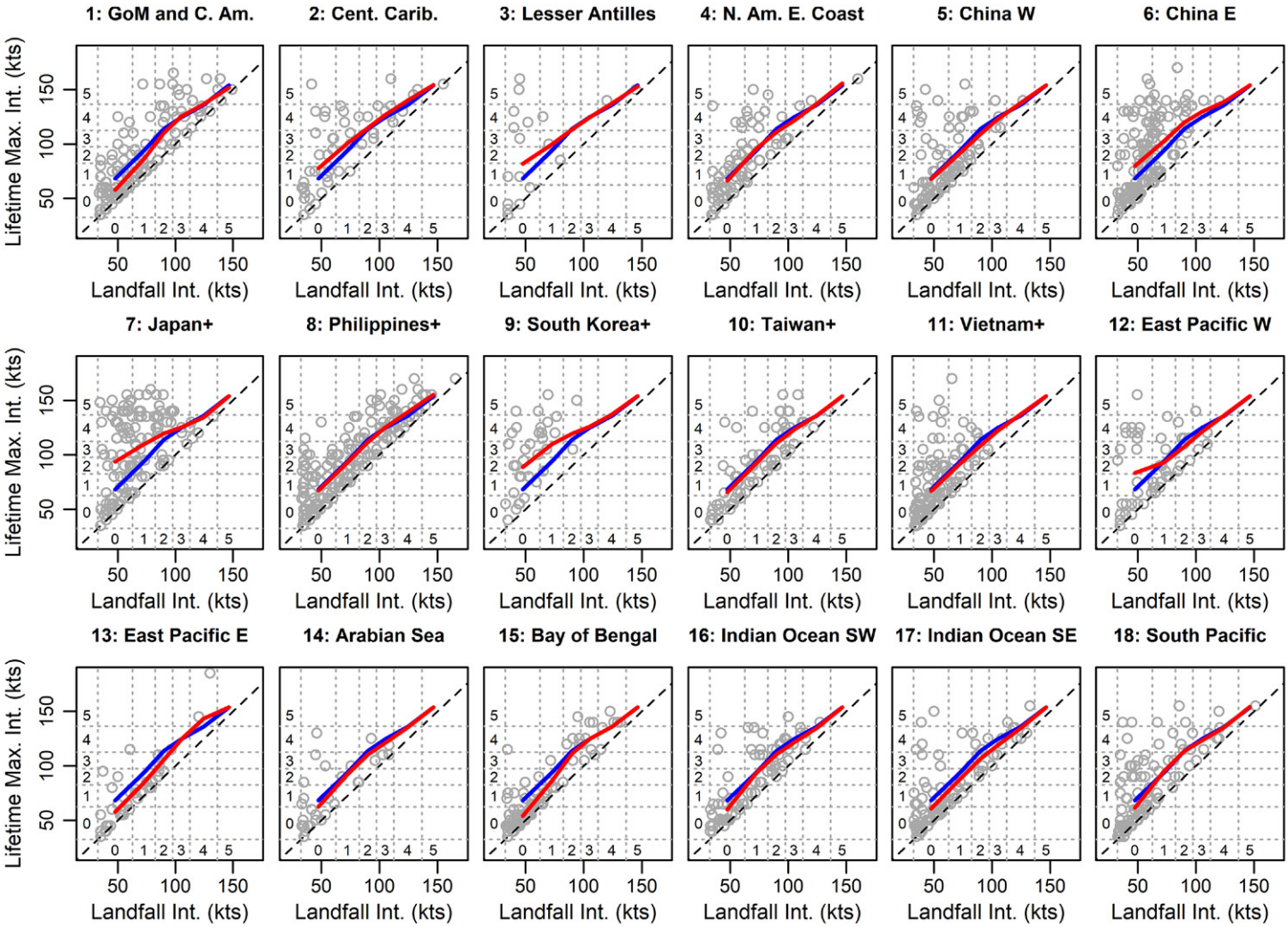

Fig. 4. Lifetime maximum intensity and landfall intensity of every landfalling storm of category 0 and above from IBTrACS, for each of the 18 regions for the period 1980–2021 (gray circles). The global expected lifetime maximum intensity (blue line, same in all panels) and the regional expected lifetime maximum intensity (red line, differs from panel to panel) are also plotted.

Implied landfall frequency changes. I can now complete my goal to derive TC frequency changes as a function of landfall intensity by region. Landfall intensity category can be converted to expected lifetime maximum intensity using the regional ELMI values, and expected lifetime maximum intensity can be converted to frequency changes using the linear model for frequency change versus lifetime maximum intensity. The result is a frequency change for every landfall intensity category in every region. Both conversion steps involve sampling from the uncertainty: the uncertainty around the ELMI curves for each region, and the uncertainty represented by the ensemble of different linear models for each basin. Because I am using a linear model for frequency versus intensity, the uncertainty does not affect the mean frequency change, but does affect the width of the distribution of frequency changes. The mathematical derivation is given in detail in appendix E. The end result of the analysis is a distribution of frequency changes for each category of storm and each region. Mean landfall frequency changes for the Bay of Bengal are shown in Fig. 1h. We see that the landfall adjustment increases the mean frequency changes at all landfall intensities, relative to the linear model. This increase is caused by the positive slope in the mean linear model interacting with the ELMI values, which are higher than the corresponding landfall intensity. Since all basins show a positive slope in the mean linear model, and the ELMI is always higher than the landfall intensity, there are increases in the mean frequency change, relative to the

linear model, for all storm categories, in all basins. In the Bay of Bengal, the increase for cat0 landfalls is relatively small. Figure 1f shows that this is because most landfalling cat0 storms had a lifetime maximum intensity of either cat0 or cat1, giving regional ELMI values that are only slightly higher than the landfall intensity. The increase in the mean frequency change for cat3 landfalls is larger. Figure 1f shows that this is because landfalling cat3 storms had lifetime maximum intensities of cat3, 4, or 5, giving a regional ELMI value somewhat higher than the landfall intensity.

Conversion to lognormal distributions. For convenience, I fit lognormal distributions to the simulations of landfall frequency change derived above so that the distribution can be summarized using two parameters. The fit of the lognormal to the simulated values is very good in all 18 cases, with average Q–Q correlations of greater than 0.99 for all basins.

Figure 1i shows the 10%–90% and 25%–75% range of frequency adjustments from the three steps of the modeling process: for the step model, for the linear model, and for the landfall model. In the landfall model results, uncertainty increases with landfall intensity. This is mainly because the underlying K2020 results show greater uncertainty for cat45 changes than for cat05 changes.

Simulation. The final results for landfall frequency changes for each region are given using 12 parameters: the location and scale parameters of 6 lognormal distributions, one for each intensity category from 0 to 5. These parameter values, along with the corresponding means and standard deviations, are given in the supporting data.

When creating simulations from these lognormal distributions, the frequency changes for different intensity categories within each region should be simulated with a rank correlation of 1, and the frequency changes for different regions within each basin should also be simulated with a rank correlation of 1. The correlation between basins has not, to my knowledge, been studied. I hypothesize that this correlation is also likely to be 1, but ideally this would be verified in some way.

Implications for landfall frequency changes

I now discuss the results from the above analysis, region by region. Mean frequencies from the step and linear models for each of the six basins are shown in Fig. 5. Mean frequency changes from the step, linear and landfall modeling for each of the 18 regions are shown in Fig. 6.

North Atlantic. In Fig. 5, the mean frequency changes in the step model show a large difference between cat03 and cat45, with decreases for cat03 and increases for cat45. This large difference leads to a steep slope in the mean linear model. As a result, although cat3 storms decrease in mean frequency in the step model, they increase in mean frequency in the linear model. As discussed above, this difference is likely to lead to large differences in estimated impacts, given the importance of cat3 storms.

In Fig. 6, the four North Atlantic regions I consider all show further increases in the mean frequencies of landfalling storms due to the landfall adjustment. For regions 2, 3, and 4 (all the Atlantic regions except the Gulf of Mexico and Central America region) all storms from cat1 to cat5 show increases in mean frequency as a result of climate change. For all four Atlantic regions the mean frequency of hurricanes (i.e., cat15 storms) increases at landfall, with increases of 6%, 11%, 11%, and 5%, respectively. The actual values of all changes shown in Figs. 5 and 6 are given in the supporting data.

Northwest Pacific. In Fig. 5, the mean frequency changes are lower than in the North Atlantic, especially for cat45. Also, the difference between the changes for cat03 and cat45, and

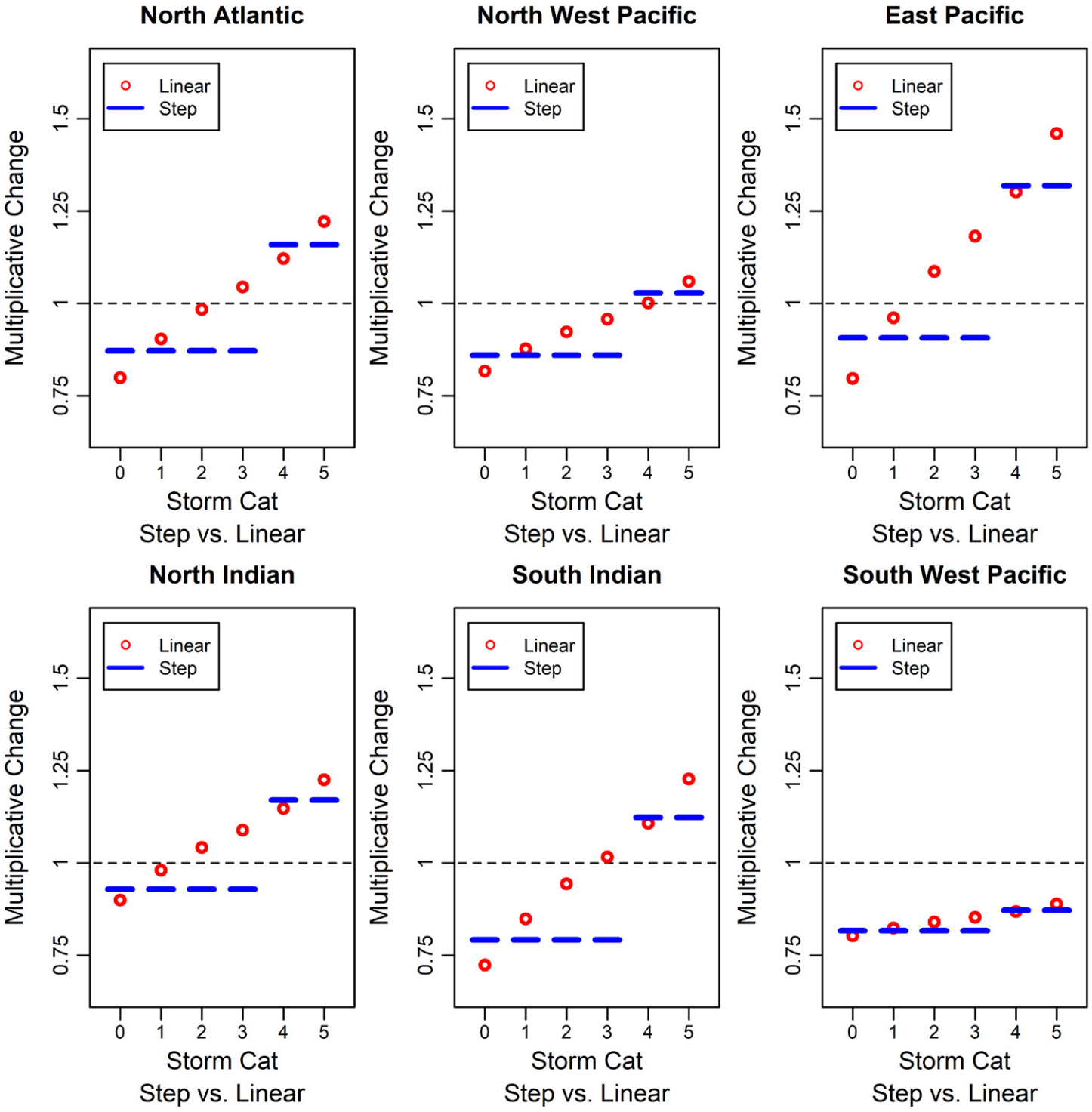

Fig. 5. Mean multiplicative changes in storm frequency vs storm intensity, for the step model (blue lines) and linear model (red circles) for all six TC basins.

hence the slope of the mean linear model, are lower. This reduces the impact of the adjustment for landfall frequencies.

Figure 6 shows the largest landfall adjustments in the Northwest Pacific basin are for China east, Japan+, and South Korea+, because of the higher values of the regional ELMI for these regions, as shown in Fig. 4.

East Pacific. In Fig. 5, the difference between the changes for cat03 and cat45 in the step model is larger than for any other basin. This leads to a large difference between the step model and linear model results, and a large impact from the landfall adjustment. The landfall

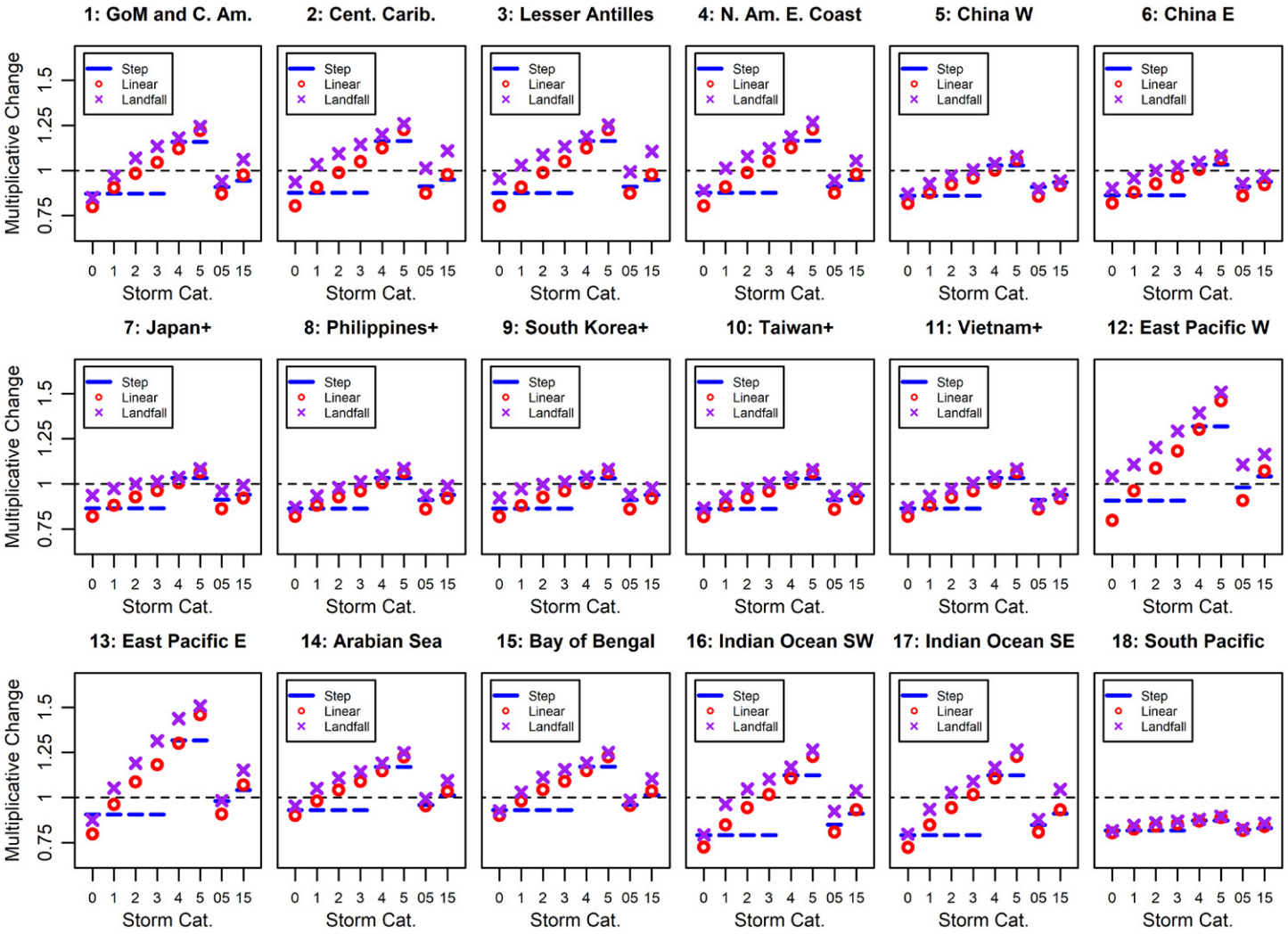

Fig. 6. Mean multiplicative changes for storm frequency, based on the step model (blue lines), linear model without landfall adjustment (red circles), and linear model with landfall adjustment (purple crosses), vs storm intensity by category, including the aggregate categories 05 and 15, for all 18 regions. The step and linear model results apply to lifetime maximum intensity, and the landfall model results apply to landfall intensity.

adjustment is rather different for the two East Pacific regions, with larger adjustments for cat01 storms for East Pacific west.

For both East Pacific regions, cat15 frequencies increase whether considered as a function of lifetime maximum intensity or landfall intensity. For the East Pacific west region, even cat05 landfalls show increasing mean landfall frequencies. The increase in cat05 frequencies arises because storms with higher lifetime maximum intensities have a higher chance of making landfall, combined with the larger increase in the frequency of storms with higher lifetime maximum intensity.

North Indian. Figure 5 shows that cat2 and cat3 storms change from decreasing mean frequency to increasing mean frequency as we move from the step to the linear model.

The landfall adjustments in Fig. 6 then show further small frequency increases. In both North Indian Ocean regions, cat15 frequencies increase for both landfall intensity and lifetime maximum intensity.

South Indian. The South Indian Ocean shows the largest projected mean decrease in cat03 frequencies. In the linear model, cat3 storms increase in mean frequency, but only by a very small margin. In both South Indian regions, landfalling cat15 frequencies increase.

Southwest Pacific. Figure 5 shows that the South Pacific is the one region where the mean frequency changes are negative for cat45. Since the changes in cat03 and cat45 are similar, the linear model is similar to the step model, and the landfall adjustment has a negligible effect.

Discussion

I have converted the K2020 TC projections into a format where they can more easily be used in TC impacts models. In particular, I have expressed them in terms of changes in frequency as a function of landfall intensity. The methods I have used involve various assumptions, such as an assumption that the regions of TC genesis and TC trajectories will not change because of climate change. Given these assumptions, I find that the changes in the mean frequencies of cat05 and cat15 storms are higher when cat05 and cat15 are defined using landfall intensities than when they are defined using lifetime maximum intensities. For the two East Pacific regions I consider, cat15 mean frequency changes show only a small increase when considered as a function of lifetime maximum intensity but show increases of 15% (±40%) and 16% (±39%) when considered as a function of landfall intensity. For the North Atlantic, North Indian, and South Indian Oceans cat15 frequency changes switch from decreases when considered as a function of lifetime maximum intensity to increases when considered as a function of landfall intensity. For the four North Atlantic regions these increases vary from 5% (±38%) to 11% (±44%); for the two North Indian regions they are 9% (±37%) and 10% (±39%); for the two South Indian Ocean regions they are both 4% (±29%). All values are given in the supporting data.

We can compare my global results with those from the hybrid climate model/statistical study by Bloemendaal et al. (2022), and my North Atlantic results with those from the climate model study by Knutson et al. (2022). Those studies, and my study, consider different metrics over different time periods, which makes quantitative comparison impossible. Qualitative comparison suggests that both the Bloemendaal et al. (2022) and the Knutson et al. (2022) results would likely fall above the mean of the distributions of change I have derived, but would lie within the range of uncertainty of my results. One particular difference is that for the Southwest Pacific, Bloemendaal et al. (2022) suggest increases in the frequency of storms, where both K2020 and I suggest decreases.

Uncertainties. It is important to emphasize that there are many sources of uncertainty involved in the analysis I have presented. Some uncertainties are quantified in the distributions used to present the results, i.e., are internal to the analysis. Others have not been quantified, i.e., are external to the analysis. In terms of external uncertainties, the results would likely be significantly different if:

- I were to repeat the K2020 multimodel analysis, but based on a different set of studies, or using weighting on the different climate model results. Some of the studies used in the K2020 analysis were based on models that can no longer be considered state of the art. A key priority is therefore to update the K2020 multimodel analysis with more recent results.
- I were to use a different source for historical TC data, such as using local agency datasets from IBTrACS rather than the U.S. Representative Agency data. As a sensitivity test, I have recalculated the results for Japan+, but using the Japanese Meteorological Agency data from IBTrACS. This has a material impact on the results, leading to lower projected frequency changes, especially for cat0 and cat1 landfalls. The results of this sensitivity test are discussed in appendixes A and D, and given in the supplemental material. Various other alternative datasets are available in IBTrACS, and may also lead to changes in results.

- I were to use a different method for interpolation versus intensity than the linear method. Interpolation has a big impact on the frequency changes for cat3 in particular.
- I were to define regions differently.
- I were to use a different method for modeling the relationship between lifetime maximum intensity and landfall intensity.

Also, the results would likely be different, but to a lesser extent, if I were to use a different parametric distribution than lognormal or if I were to use a different time period for the historical TC data.

Because of these various uncertainties, it is possible that actual future climate outcomes will lie in the tails of the distributions given by my projections. The distributions of internal uncertainty show that I cannot even be confident of the signs of changes in the mean, and future studies may well show results that are qualitatively different in that respect, i.e., where I show increases in the mean, future studies may show decreases, and vice versa. Future studies may also show different relativities between the results for different basins and between different regions, i.e., where I am projecting larger changes in region A than in region B, future studies may show the opposite.

In addition to the uncertainties, a shortcoming of my analysis is that I have only considered changes in landfall frequency of TCs as driven by changes in the frequency of TCs as a function of lifetime maximum intensity. TC landfall frequencies may be changing for other reasons too, some of which may be more important, including changes in genesis regions and trajectories.

Furthermore, I have only considered changes in landfall frequency. Mean intensity changes can be derived from the frequency changes I present, but I have not considered possible changes in other TC parameters, such as forward speed and size, which may also lead to changes in impacts. How TC characteristics may change remains one of the least well understood aspects of climate change, and there is much more work that needs to be done at all levels. That includes developing a better understanding of the fundamental physics, and using higher-resolution and more realistic climate models. For instance, as an example of where climate models may be failing to simulate realistic climate in a way that may be relevant for TC projections, it has recently been suggested that climate models may not be simulating zonal gradients in Pacific equatorial sea surface temperatures correctly (Lee et al. 2022). Further work should also include extracting more information from existing climate model output and improving the practical application of existing information to impacts models.

In spite of the uncertainties and shortcomings in my study, I hope that the results I present can provide a useful ready-to-use set of projections for changes in TC landfalling frequencies under climate change. The projections can be updated as our understanding progresses. I also hope that this work, and the challenges I have identified with respect to applying climate model outputs in impacts models, can lead to developments in terms of what information is extracted from climate models in the future.

Acknowledgments. I am grateful to Tom Knutson for various discussions on these topics, and to Chris Landsea, Phil Klotzbach, and the two anonymous reviewers for their suggestions.

Data availability statement. Various datasets from this study are available as supporting data at Jewson (2022c).

Appendix A: Data

K2020 tropical cyclone projections. I consider the K2020 projections for changes in the frequency of cat05 and cat45 storms. The projections consist of a minimum value, five quantiles, and a maximum value, corresponding to a 2°C increase in global mean surface temperature. I ignore the minimum and maximum values and consider only the five quantiles. For cat05 storms, the quantiles are 5%, 25%, 50%, 75%, and 95%, while for cat45 storms, they are 10%, 25%, 50%, 75%, and 90%. The values are illustrated in K2020, Figs. 1 and 2.

In my analysis I also consider frequency changes for cat0 storms (reported maximum one minute sustained wind-speeds in the range 34–63 kt), cat1 storms (64–82 kt), cat2 storms (83–95 kt), cat3 storms (96–112 kt), cat4 storms (113–136 kt), and cat5 storms (over 136 kt).

IBTrACS historical TC data. The historical TC data I use are a subset of the IBTrACS dataset (Knapp et al. 2010). IBTrACS contains one or more estimates of TC characteristics for each historical storm, as produced by different weather agencies. For consistency, I use the intensity estimates referred to as the "U.S. Representative Agency" data. These data are from the National Hurricane Center for the North Atlantic and East Pacific, the Central Pacific Hurricane Center for the central North Pacific and the Joint Typhoon Warning Center for the remainder of the Pacific Ocean and the Indian Ocean. I follow the IBTrACS dataset definitions for the dividing lines between basins, which are, for the Northwest Pacific and East Pacific, longitude 180°, and for the South Indian Ocean and Southwest Pacific, longitude 135°E. I use data from 1980 to 2021, since global coverage from geostationary and polar-orbiting satellites was available during this period. For each storm, I extract the single value that gives the maximum intensity of the storm within the basin, and linearly interpolate the intensities from the points immediately before and after landfall to estimate intensity at landfall.

As a sensitivity test, I have also recalculated all results, but replacing the "U.S. Representative Agency" data with the data labeled "Tokyo" in IBTrACS, which are Japanese Meteorological Agency (JMA) data, for Japan+ landfall only. I multiplied the intensities in the JMA data by 1.12, to account for the difference between 10- and 1-min sustained winds.

Appendix B: Fitting distributions, correlations, and deriving cat03 changes

J2022a considered the question of how to fit distributions to the K2020 quantiles for cat05, cat45, and mean intensity. They used a somewhat complex scheme to fit distributions in such a way that the changes in frequency and mean intensity were consistent. They found that consistency between the frequency and mean intensity changes could only be achieved by using correlations of 1 between the three variables. I therefore also adopt a correlation of 1 between the changes in cat05 and cat45 frequencies in my analysis.

J2022a also found that the changes in frequency and mean intensity represent essentially the same information, and that the distributions of changes in mean intensity can be derived from the distributions of changes in frequency. Based on this result, I consider only the changes in frequency from K2020. Changes in mean intensity can be derived from the changes in frequency if required.

The J2022a methodology for fitting distributions to changes in cat05 frequency, cat45 frequency, and mean intensity adjusted the fitted distributions for all three variables simultaneously, taking into account the mathematical relationship between frequency and mean intensity which arises from the definition of mean intensity. This methodology is instructive for understanding the relationship between changes in frequency and mean intensity, and for deriving the implied correlation between frequency and mean intensity, but is cumbersome for general usage. I therefore use a simpler methodology, and fit distributions to the two frequency variables separately. I use lognormal distributions and an iterative scheme that chooses the distribution parameters that minimize the mean squared distance

between the given and fitted quantiles. The values of the fitted parameters are given in the supporting data.

Given distributions for fractional changes in cat05 and cat45, with a correlation of 1 between the distributions, I derive a distribution for the fractional changes in cat03 frequencies using historical storm frequencies extracted from IBTrACS. The derivation has three stages. First, TC frequencies are used to convert the fractional changes in the frequency of cat05 and cat45 storms into changes in absolute numbers of cat05 and cat45 storms. Second, these changes in the absolute numbers of cat05 and cat45 storms are used to calculate changes in absolute numbers of cat03 storms. Finally, these changes in the absolute number of cat03 storms are then converted to fractional changes in numbers of cat03 storms. For convenience, I fit a lognormal distribution to the resulting cat03 values. The values of the fitted parameters are given in the supporting data. The goodness of fit for the Bay of Bengal is illustrated in Fig. 1c and for other basins in the supplemental material. The fit is good for all six basins, with all six Q–Q correlations being above 0.995.

Appendix C: Regionality in the relationship between lifetime maximum intensity and landfall intensity

The relationship between lifetime maximum intensity and landfall intensity was discussed in J2022b, in the context of the step model for frequency versus intensity for the North Atlantic. J2022b investigated the relationship between lifetime maximum intensity and landfall intensity using the variable pwas45, defined as the probability that a landfalling storm was previously cat45. They showed that HURDAT2 data (Landsea and Franklin 2013) for the North Atlantic suggest that pwas45 for cat03 storms varies in space within the North Atlantic basin: in some landfall regions, most landfalling cat03 storms were previously cat45, i.e., pwas45 is high. In other regions, most landfalling cat03 storms were not previously cat45, i.e., pwas45 is low. This shows that the relationship between lifetime maximum intensity and landfall intensity is best quantified on a regional basis in some way. J2022b also showed that pwas45 varies with landfall intensity, as would be expected. They divided the North Atlantic basin into four landfall regions based on the properties of historical storms, and modeled pwas45 as a function of landfall intensity in each region using a logistic regression model. These results motivate me to define regions for the present study that can help capture the spatial variation in the relativity between lifetime maximum intensity and landfall intensity.

For the North Atlantic, I use the regions defined by J2022b. For the other basins, I define regions subjectively based on four factors:

- The need for each region to contain enough historical landfalls that landfall adjustments can be estimated.
- An assessment of whether there are spatial variations in the relationship between lifetime maximum intensity and landfall intensity. Following the method from J2022b, as described above, this assessment involves plotting all cat03 landfalls for the region, with an indication of whether their lifetime maximum intensity was cat03 or cat45. Regions are then defined to capture regions in which the proportion of landfalling cat03 storms that were previously cat45 is relatively constant in space. I call this pwas45 analysis. The figures on which it is based are given for all 18 regions in the supplemental material.
- An assessment of whether there may be spatial variations in the relationship between lifetime maximum intensity and landfall intensity based on geographical and climatological factors.
- Political boundaries.

The regions are illustrated in Fig. 2. I split the Northwest Pacific basin into six regions based on political boundaries with extensions: China, Japan+, Philippines+, South Korea+, Taiwan+, and Vietnam+. I then split China into two regions, because China experiences a large number of landfalling TCs over a wide area, and the pwas45 analysis suggests that there are differences in landfall characteristics within that large area.

For the East Pacific basin, I split into two regions: the first consists of Hawaii and the more northerly portion of the west coast of North America. The second consists of the more southerly portion of the west coast of North America, a region in which the pwas45 analysis suggests that pwas45 may be lower.

For the North Indian Ocean, I split into two regions: the Arabian Sea and the Bay of Bengal, on the basis that the climatological behavior in these two regions is different. The pwas45 analysis suggests that the southeast coast of India and Sri Lanka may have a lower pwas45 than the northeast coast of India, Bangladesh, and Myanmar. This would be consistent with the general observation that pwas45 tends to be lower near the equator, as can be seen by considering the various figures in the supplemental material. However, I do not subdivide the region further because the data in the subregions would become too sparse.

For the South Indian Ocean, I split into two regions: the western portion (where most landfalls are in Madagascar and Africa) and the eastern portion (where most landfalls are in Australia), because climatological behavior in these two regions is very different.

For the South Pacific Ocean, I use just one region because of the sparsity of data, although there are perhaps indications in the pwas45 analysis that pwas45 is lower for landfalls in the Gulf of Carpentaria.

Further research, either using observations or models, may be able to shed more light onto the question of how pwas45 and the relationship between lifetime maximum intensity and landfall intensity varies in space in various parts of the world.

I extend my region definitions so that in aggregate they cover almost everywhere that a TC might possibly be expected to occur, including regions with few historical storms. This extension has no material effect on my modeling of frequency changes but is to allow the regions to be used in impacts models which require region definitions that account for every possible storm that might occur in the future, or that might occur in a TC simulation model.

Appendix D: Lifetime maximum and landfall intensity modeling

J2022b used a logistic regression model to capture the relationship between lifetime maximum intensity and landfall intensity in four North Atlantic regions. They were able to use logistic regression because when using the step model, the only input required to determine the frequency change for a storm is whether that storm had a lifetime maximum intensity of cat03 or cat45. However, in the present study the modeling problem is more complex because I am using the linear model, which requires storm lifetime maximum intensity in knots as input. It may be possible to develop a generalization of the logistic regression model to solve this more complex problem. Such a model could allow for landfall adjustments based on landfall intensity and lifetime maximum intensity, both in knots. However, creating such a model may not be justified or necessary given the uncertainties in the K2020 projections.

Instead, I use a simple nonparametric approach for understanding the relationship between lifetime maximum intensity and landfall intensity. My approach is straightforward to understand and implement. First, I simplify the modeling challenge by seeking to quantify the frequency changes only for each landfall intensity category (six categories, from 0 to 5), rather than continuously as a function of landfall intensity in knots. This also has the benefit of simplifying the outputs of the whole study, which I then report by landfall intensity category.

Second, I pool the data for all regions and calculate the mean lifetime maximum intensity using historical storms in each landfall intensity category. I call this mean the global ELMI. The ELMI gives an indication, globally, of what lifetime maximum intensity landfalling cyclones of different intensities would typically have had on average. Values of the global ELMI are given in Fig. 3. For cat0 landfalls the ELMI is in the middle of the cat1 intensity range; for cat1 landfalls it is on the boundary between cat2 and cat3; for cat2 landfalls it is at the low end of the cat4 range; for cat3 landfalls it is at the high end of the cat4 range; for cat4 landfalls it is at the low end of the cat5 range and for cat5 landfalls it is about 20 kt into the cat5 range.

Third, I calculate regional values of the ELMI. Because the data are sparse in some landfall regions for some landfall intensity categories, simply calculating the average of the lifetime maximum intensities of the storms in each landfall intensity category leads to irregular values for the regional ELMI. To overcome this irregularity in the results I blend the average of the lifetime maximum intensities for each region and landfall category with the global ELMI values. I also smooth the results. In the blending step, the regional ELMI is calculated as the weighted combination of the global ELMI and the average of the lifetime maximum intensities for that region for that landfall intensity. The weight on the global ELMI is equal to one over the square root of one plus the number of storms in that region/landfall category. When there are no storms in the region/category, this puts all of the weight on the global ELMI, while when there are many storms in the region/category this puts almost all the weight on the regional data. In the smoothing step, I then adjust the regional ELMI values for cat1, 2, 3, and 4 storms so that the regional ELMI versus storm intensity moves closer to linear. For example, to smooth cat1 values I use the regional ELMI values for cat0 and cat2 to define a straight line, as a function of intensity. I then perform a 50–50 weighted average between the unsmoothed cat1 value and the straight line, to derive a new smoothed cat1 value. The blending and smoothing adjustments produce results that are plausibly regular, but that still capture the regional variations in the ELMI. I also calculate the standard error uncertainty around the regional ELMI values, as a function of the number of data points.

For Japan+, I have recalculated implied landfall frequencies using "Tokyo" data, i.e., JMA data, from IBTrACS. Alternative versions of Figs. 4 and 6 are given in the supplemental materials. Many storms in the JMA data have lower lifetime maximum intensities, and this leads to lower landfall adjustments. This has a big impact on the projected frequencies of cat0 and cat1 storms, a smaller impact on the projected frequencies of cat2 and cat3 storms, and no impact on the projected frequencies of cat4 and cat5 storms.

Appendix E: Mathematical derivation of the landfall conversion methodology

The method for conversion to landfall frequencies can be derived as follows. I define the baseline numbers of TCs in terms of lifetime maximum intensity and in terms of landfall frequency as m and n, respectively. I define the same but after adjustment for climate change as m' and n'. I define the landfall category as c and the lifetime maximum intensity as x. The multiplicative change in landfall frequencies that I want to calculate is then given by $E(n'|c)/E(n|c)$. Using the law of total expectation, this can be written as $E_c[E(n'|c,x)]/E_c[E(n|c,x)]$, where the expectation E_c represents an expectation over x, with c constant. This shows that I can calculate the changes in landfall frequency for fixed lifetime maximum intensity first, and then average those changes over different lifetime maximum intensities.

I then assume that frequency as a function of landfall intensity changes in proportion to changes in frequency as a function of lifetime maximum intensity, which I write as

$E(n|c, x) = p(x, c)E(m|x)$ and $E(n'|c, x) = p(x, c)E(m'|x)$. The constant of proportionality $p(x, c)$ can vary with x and c, but is assumed not to change because of climate change. In meteorological terms, this implicitly assumes that regions of genesis and trajectories remain constant. This gives

$$\frac{E\left(n'\middle|c\right)}{E\left(n\middle|c\right)}=\frac{E_c\left[E\left(n'\middle|c,x\right)\right]}{E_c\left[E\left(n\middle|c,x\right)\right]}=\frac{E_c\left[p\left(x,c\right)E\left(m'\middle|c,x\right)\right]}{E_c\left[p\left(x,c\right)E\left(m\middle|c,x\right)\right]}=\frac{E_c\left[p\left(x,c\right)\right]E_c\left[E\left(m'\middle|c,x\right)\right]}{E_c\left[p\left(x,c\right)\right]E_c\left[E\left(m\middle|c,x\right)\right]}=\frac{E_c\left[E\left(m'\middle|c,x\right)\right]}{E_c\left[E\left(m\middle|c,x\right)\right]},$$

which shows how we can express changes in frequencies as a function of landfall intensity in terms of changes in frequency as a function of lifetime maximum intensity. The linear model is a model for $E(m'|x,c)/E(m|x,c)$, and gives $E(m'|x,c)/E(m|x,c)=\alpha+\beta x$. Combining these expressions gives

$$\frac{E\left(n'\middle|c\right)}{E\left(n\middle|c\right)}=\frac{E_c\left[\left(\alpha+\beta x\right)E\left(m\middle|c,x\right)\right]}{E_c\left[E\left(m\middle|c,x\right)\right]}=\frac{E_c\left[\left(\alpha+\beta x\right)\right]E_c\left[E\left(m\middle|c,x\right)\right]}{E_c\left[E\left(m\middle|c,x\right)\right]}=\alpha+\beta E_c\left(x\right)=\alpha+\beta E\left(x\middle|c\right),$$

where $E(x|c)$ is the ELMI. This equation gives the mean multiplicative frequency changes, which are illustrated by the means of the third bar of each set in Fig. 1i. In this equation, α and β are uncertain, because they are derived from the K2020 results, and $E(x|c)$ is uncertain, as shown in Fig. 1g, because it is estimated from the IBTrACS data for intensities. I sample from the distributions of uncertainty for α, β, and $E(x|c)$ and recompute $\alpha+\beta E(x|c)$ a large number of times to give the distributions of multiplicative frequency changes, which are illustrated by the ranges of the third bar of each set in Fig. 1i. The sampling of α, β, and $E(x|c)$ propagates both the K2020 uncertainty and the landfall conversion uncertainty into the results.

References

Bai, L., Y. Xu, J. Tang, and R. Guo, 2023: Interagency discrepancies in tropical cyclone intensity estimates over the western North Pacific in recent years. *Atmos. Sci. Lett.*, **24**, e1132, https://doi.org/10.1002/asl.1132.

Bhatia, K., G. Vecchi, T. Knutson, H. Murakami, J. Kossin, K. Dixon, and C. Whitlock, 2019: Recent increases in tropical cyclone intensification rates. *Nat. Commun.*, **10**, 3942, https://doi.org/10.1038/s41467-019-11922-2.

Bloemendaal, N., and Coauthors, 2022: A globally consistent local-scale assessment of future tropical cyclone risk. *Sci. Adv.*, **8**, eabm8438, https://doi.org/10.1126/sciadv.abm8438.

Chen, W., Y. Lu, S. Sun, Y. Duan, and G. Leckebusch, 2018: Hazard footprint-based normalization of economic losses from tropical cyclones in China during 1983–2015. *Int. J. Disaster Risk Sci.*, **9**, 195–206, https://doi.org/10.1007/s13753-018-0172-y.

Colbert, A., B. Soden, G. Vecchi, and B. Kirtman, 2013: The impact of anthropogenic climate change on North Atlantic tropical cyclone tracks. *J. Climate*, **26**, 4088–4095, https://doi.org/10.1175/JCLI-D-12-00342.1.

Emanuel, K., 2020: Response of global tropical cyclone activity to increasing CO_2: Results from downscaling CMIP6 models. *J. Climate*, **34**, 57–70, https://doi.org/10.1175/JCLI-D-20-0367.1.

Garner, A., R. Kopp, and B. Horton, 2021: Evolving tropical cyclone tracks in the North Atlantic in a warming climate. *Earth's Future*, **9**, e2021EF002326, https://doi.org/10.1029/2021EF002326.

Hassanzadeh, P., C. Lee, E. Nabizadeh, S. Camargo, D. Ma, and L. Yeung, 2020: Effects of climate change on the movement of future landfalling Texas tropical cyclones. *Nat. Commun.*, **11**, 3319, https://doi.org/10.1038/s41467-020-17130-7.

Jewson, S., 2021: Conversion of the Knutson et al. tropical cyclone climate change projections to risk model baselines. *J. Appl. Meteor. Climatol.*, **60**, 1517–1530, https://doi.org/10.1175/JAMC-D-21-0102.1.

——, 2022a: The interpretation and implications of the Knutson et al. 2020 projections of changes in the frequency and intensity of tropical cyclones under climate change. *Quart. J. Roy. Meteor. Soc.*, **148**, 2219–2242, https://doi.org/10.1002/qj.4299.

——, 2022b: Conversion of the Knutson et al. tropical cyclone frequency projections to North Atlantic landfall. *J. Appl. Meteor. Climatol.*, **61**, 1419–1432, https://doi.org/10.1175/JAMC-D-22-0056.1.

——, 2022c: Supplemental data for the paper "Tropical Cyclones and Climate Change: Global Landfall Frequency Projections Derived from Knutson et al." Zenodo, accessed 14 May 2023, https://doi.org/10.5281/zenodo.7090197.

Knapp, K., M. Kruk, D. Levinson, H. Diamond, and C. Neumann, 2010: The International Best Track Archive for Climate Stewardship (IBTrACS): Unifying tropical cyclone best track data. *Bull. Amer. Meteor. Soc.*, **91**, 363–376, https://doi.org/10.1175/2009BAMS2755.1.

Knutson, T., and Coauthors, 2020: Tropical cyclones and climate change assessment: Part II: Projected response to anthropogenic warming. *Bull. Amer. Meteor. Soc.*, **101**, E303–E322, https://doi.org/10.1175/BAMS-D-18-0194.1.

——, J. Sirutis, M. Bender, R. Tuleya, and B. Schenkel, 2022: Dynamical downscaling projections of late twenty-first-century U.S. landfalling hurricane activity. *Climatic Change*, **171**, 28, https://doi.org/10.1007/s10584-022-03346-7.

Landsea, C., and J. Franklin, 2013: Atlantic hurricane database uncertainty and presentation of a new database format. *Mon. Wea. Rev.*, **141**, 3576–3592, https://doi.org/10.1175/MWR-D-12-00254.1.

Lee, S., M. L'Heureux, A. Wittenberg, R. Seager, P. O'Gorman, and N. Johnson, 2022: On the future zonal contrasts of equatorial Pacific climate: Perspectives from observations, simulations, and theories. *npj Climate Atmos. Sci.*, **5**, 82, https://doi.org/10.1038/s41612-022-00301-2.

Liu, M., G. Vecchi, J. Smith, and T. Knutson, 2019: Causes of large projected increases in hurricane precipitation rates with global warming. *npj Climate Atmos. Sci.*, **2**, 38, https://doi.org/10.1038/s41612-019-0095-3.

Martinez, A., 2020: Improving normalized hurricane damages. *Nat. Sustainability*, **3**, 517–518, https://doi.org/10.1038/s41893-020-0550-5.

Murakami, H., T. Delworth, W. Cooke, M. Zhao, B. Xiang, and P. Hsu, 2020: Detected climatic change in global distribution of tropical cyclones. *Proc. Natl. Acad. Sci. USA*, **117**, 10706–10714, https://doi.org/10.1073/pnas.1922500117.

Stansfield, A., K. Reed, and C. Zarzycki, 2020: Changes in precipitation from North Atlantic tropical cyclones under RCP scenarios in the variable-resolution Community Atmosphere Model. *Geophys. Res. Lett.*, **47**, e2019GL086930, https://doi.org/10.1029/2019GL086930.

Sun, Y., and Coauthors, 2017: Impact of ocean warming on tropical cyclone size and its destructiveness. *Sci. Rep.*, **7**, 8154, https://doi.org/10.1038/s41598-017-08533-6.

Weinkle, J., C. Landsea, D. Collins, R. Musulin, R. Crompton, P. Klotzbach, and R. Pielke Jr., 2018: Normalized hurricane damage in the continental United States 1900–2017. *Nat. Sustainability*, **1**, 808–813, https://doi.org/10.1038/s41893-018-0165-2.

Yamaguchi, M., J. Chan, I. Moon, K. Yoshida, and R. Mizuta, 2020: Global warming changes tropical cyclone translation speed. *Nat. Commun.*, **11**, 47, https://doi.org/10.1038/s41467-019-13902-y.

Zhang, G., H. Murakami, T. Knutson, and K. Yoshida, 2020: Tropical cyclone motion in a changing climate. *Sci. Adv.*, **6**, eaaz7610, https://doi.org/10.1126/sciadv.aaz7610.